Diamond & Related Materials 146 (2024) 111214

Contents lists available at ScienceDirect

Diamond & Related Materials

journal homepage: www.elsevier.com/locate/diamond

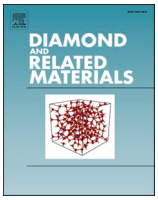

Study on heat-treated pyrolytic carbon deposited from methane on directly heated carbon fibres

Ryszard Wielowski [a], Paweł Czaja [b], Wojciech Piekarczyk [a], Marcel Zambrzycki [a], Maciej Gubernat [a], Aneta Fraczek-Szczypta [a,*]

[a] Faculty of Materials Science and Ceramics, AGH University of Krakow, Mickiewicza 30 Av., 30-059 Krakow, Poland
[b] Institute of Metallurgy and Materials Science, Polish Academy of Science, Reymonta 25 St., 30-059 Krakow, Poland

ARTICLE INFO

Keywords:
Pyrolytic carbon
Pyrocarbon
Carbon fibre
C/C composites
Heat treatment
CVD

ABSTRACT

The study investigated the morphology, microstructure, structure, texture, and mechanical properties of heat-treated at 1600 °C and 2000 °C pyrolytic carbon (PyC) deposited from methane using various methods such as scanning electron microscopy (SEM), X-ray diffraction (XRD), high-resolution transmission electron microscopy (HRTEM), selected area electron diffraction (SAED), Raman spectroscopy, and ultrasonic dynamic measurements of Young's modulus. The PyC was synthesised at 1100 °C using a chemical vapour deposition (CVD) method with direct electrical heating of the two types of carbon fibres (CFs). The results showed that the PyC had a low- and medium-texture (LT and MT PyC). Analysis of the graphitization trajectory allowed the determination of structural changes in the material as a function of temperature, including the growth of crystallites and an increase in the crystallinity proportion without the significant rearrangement within PyC. The crystallite size and the number of interstitial defects has increased with temperature that controlled mechanical properties. Therefore, based on the results obtained, the most suitable composites for further research in the context of electrodes for stimulation of nervous tissue were obtained at the temperature of their synthesis, i.e. at 1100 °C.

1. Introduction

The first discovery of pyrolytic carbon (PyC) was probably in 1961 and resulted from work on the formation of a carbon film from carbon suboxides [1]. PyC has been of increasing research interest in various aspects, during the late 1960s and early 1970s, continuing into the 1980s. The development and commercialization of PyC for heart valve prostheses in the late 1960s marked a significant milestone [2]. Additionally, the 1980s witnessed advances in the understanding of the structure of PyC, its properties, and processing techniques [3–7]. These advances were driven by development of varied applications, including aerospace [8,9] (which often overlaps with military technology due to similar material requirements), nuclear [9,10], electrical [9], and even medical [9,11,12] applications.

Originally, PyC was produced through a fluidized bed chemical vapour deposition (FBCVD) process [13,14]. This technique involved pyrolysis, leading to the creation of PyC with various microstructures [15]. Along with CVD techniques, the chemical vapour infiltration (CVI) method has evolved, opening new possibilities for producing composites, particularly carbon-carbon (C/C) [16]. The state-of-the-art approach to obtaining PyC in a C/C composite is electrical (resistance) heating of a bundle of carbon fibres and direct deposition of pyrolytic carbon [17–19]. This approach was first presented in 2018 [18], and since last year a new variant of the CVD method has been developed using direct bundle heating, which reduces the time from a multi-hour process to a few minutes [19]. The choice of synthesis parameters, such as times, gas concentrations and fibre types, and especially the heating temperature, is extremely important.

In general, the pyrolysis reaction of light hydrocarbons often requires a minimum temperature (800–1200 °C) [20–23]. It is a highly endothermic process with positive Gibbs free energies until a temperature of 1027 °C is reached, and the aromatic hydrocarbons are more thermodynamically favoured with increasing temperature [24], including obtaining favourable kinetics [25]. However, pyrolysis simultaneously involves radical dehydrogenation towards the formation of small clusters [25]. This is related to the fact that hydrogen radical

* Corresponding author at: Mickiewicza 30 Av., 30-059 Krakow, Poland.
E-mail addresses: rwielows@agh.edu.pl (R. Wielowski), czaja.p@imim.pl (P. Czaja), wpiekar@agh.edu.pl (W. Piekarczyk), zambrzycki@agh.edu.pl (M. Zambrzycki), guma@agh.edu.pl (M. Gubernat), afraczek@agh.edu.pl (A. Fraczek-Szczypta).

https://doi.org/10.1016/j.diamond.2024.111214
Received 25 March 2024; Received in revised form 6 May 2024; Accepted 17 May 2024
Available online 20 May 2024

reactions have lower energy barriers than direct decomposition and recrystallisation reactions. The C—H bond, which is the highest energy barrier (104 kcal/mol), is dissociated by the hydrogen radical at 927 °C [20,25]. In the initial contact with the substrate, carbon chains (clusters) and early carbon ring deposits are formed from the precursor gas. Subsequently, larger PAHs are deposited on the substrate, where a more regular 3D carbon structure is formed [26]. At higher temperatures and concentrations, the equilibrium constant for such endothermic reactions will therefore be increased, favouring the formation and deposition of larger particles of PAHs, from which soot can be deposited, rather than single carbon linear particles [26,27].

Nevertheless, depending on the processing conditions and subsequent thermal treatment, PyCs may have different properties due to structural and textural differences. At lower temperatures, the materials had an isotropic and/or granular structure, while at higher temperatures, they exhibited a more laminar structure. There is a tendency towards a preferred orientation along the (002) plane, and the crystallite size increased in line with rising temperature of heat treatment [28,29]. Some recent reports do not confirm such a correlation for higher values of mechanical parameters [30,31] or degrees of disorder [27].

Differences would have to be found in the structure and texture of PyC treated at temperatures higher than those used. In the case of graphitized PyC layers, an increase in temperature treatment (2000–3000 °C) accelerates the ordering processes and large changes in size and elemental cells occur [21,32]. For PyC synthesised from methane at temperatures of 1350 °C and above, additional heating at significantly lower temperatures of 1700 °C [15] and 1900 °C [33] resulted in changes in the structure of the materials obtained.

The application of the CVD method with direct heating of the fibre bundle has been optimised and described in previous work [19]. However, the effect of the type of carbon fibre used on the PyC matrix obtained has not been considered to date. Focusing on the structure of such a substrate, one should lean towards acknowledging a partial influence on the formation of PyC layers obtained under the same conditions. The microstructure and morphology [34,35], as well as the crystallographic ordering [36] of the substrate have already been attributed to the influence of the texture of the deposited PyC. Thus, the use of carbon fibres with different degrees of graphitization may affect the PyC matrix achieved. Therefore, it can be concluded that substrates with a hexagonal structure, like graphite, will promote the growth of layers of larger aromatic hydrocarbons (fewer active edges than for less ordered carbon materials). The pattern of the formation of the further layers will therefore depend on the concentration and type of gaseous precursors, the deposition of linear C_2 and aromatic (benzene and PAHs) molecules and this should be attributed to chemisorption and/or adsorption processes [37], temperature, and synthesis time.

These findings contribute to the understanding of how processing conditions and thermal treatment can impact the properties of pyrolytic carbons, including morphology, structure, texture, and their mechanical properties, especially at lower pyrolysis temperatures using CVD methods with direct heating of the bundle.

The changes and differences identified will improve the final composite. It should be noted that ongoing research into the use of pyrolytic carbon layers on carbon fibre as C/C composites, among other carbon materials [38], in contact with nervous tissue [19], is an innovative direction in the field of medical applications. Knowledge of the elementary nature of the PyC layers will allow for more advanced in vitro and electrochemical studies.

In this study, the impact of additional thermal treatment on the morphological, structural, and textural characteristics of individual phases (carbon fibres - CF and pyrolytic carbon - PyC) and their composites (CF/PyC) was assessed through an advanced version of the chemical vapour deposition (CVD) technique. Scanning electron microscopy (SEM) analyses enabled the evaluation of the microstructure of the produced samples, including the extent of pyrocarbon (PyC) filling within the fibre bundle. A crucial factor influencing the functional properties of the resulting composites is the structure of pyrolytic carbon, which was examined using techniques such as high-resolution transmission electron microscopy (HRTEM), selected area electron diffraction (SAED), Raman spectroscopy, and X-ray diffraction (XRD). The fibres and composites were further characterised by measuring the dynamic Young's modulus via ultrasonic methods. We believe that this work will contribute to narrowing the gaps in research on pyrolytic carbon produced by CVD methods with direct heating of the bundle. Thus, it will unequivocally clarify uncertainties that have not been clearly addressed in the literature. It is also hoped that it will further advance the study of C/C composites in the form of carbon fibre-based microelectrodes and PyC for the stimulation of nerve tissue to help sufferers of neurodegenerative diseases such as Alzheimer's, ALS, or Parkinson's.

2. Experimental

2.1. Materials

The composite materials acquired in the experiment were based on two types of PAN (polyacrylonitrile) precursor carbon fibre (CF): high-modulus CF-G (GY80, Celanese Co.) and low-modulus CF-S (Sigrafil, SGL Carbon SE). Characteristic parameters from the CFs' technical data sheet are presented in Table 1.

The carbon fibres used have different shapes of cross-section: a dog-bone-like (GY80) and a kidney-bean-like (Sigrafil) shape. These shapes are characteristic of carbonized fibres from PAN, and these differences between CFs are illustrated in Figs. 1 and 4. Carbonized (low-graphitized) CFs, like Sigrafil, are obtained at typical temperatures for low-modulus fibres in the range of 1200–1600 °C. They are characterised by a more organised outer layer and a highly disordered interior composed of pseudo-crystalline packets with dimensions of several nanometres [39]. Characteristic microscopic separations from PAN after carbonization are also observable in the fibre core. A different morphology is exhibited by GY80, characteristic of high-modulus fibres manufactured from PAN. CF-G is categorised as a partially graphitized fibres, with a characteristic receiving temperature in the range of 2000–3000 °C. They have the structure of turbostratic carbons, and the structural units are complex and entangled parallel to the fibre axis with dimensions of tens of nanometres [40]. No differences in structure are shown between the core and the outer layer of the fibre.

Carbon-carbon (C/C) composite matrix was synthesised from carbonous precursor methane and diluted with nitrogen as an inert gas. The inert atmosphere in further thermal treatment was provided by argon gas (gases from LiquidAir SA, purity of 99.999 %).

2.2. Fabrication

The chemical vapour deposition (CVD) method with direct electrical heating of carbon fibres was conducted in a device called CFCPP-1100, Carbon Fiber Pyrolytic Carbon Coating, by Fine Instruments, Poland. A detailed description of the equipment installation and the general scheme of the CF/PyC composite samples preparation is described in our previous publication [19]. In the experiment, 30 samples each of CF/PyC composites based on CF-S and CF-G fibres were produced at a temperature range of 1100–1140 °C. For synthesis purposes, a bundle of CF-S weighing 0.51 ± 0.06 mg, or CF-G weighing 0.72 ± 0.07 mg, which

Table 1
Comparison of the parameters of the carbon fibres.

Type of CF	Density [g/cm^3]	Tensile strength [GPa]	Tensile modulus [GPa]	Number of filaments in a roving [−]	Tex [g/km]
CF-G	1.96	1.86	572	250	
CF-S	1.80	4.0	240	50,000	3420

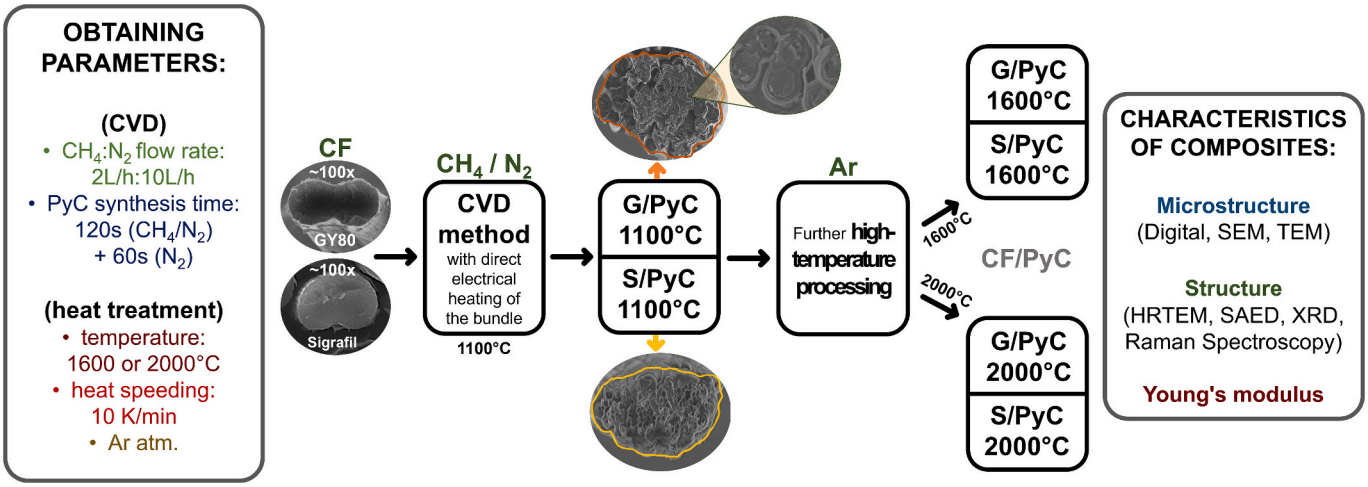

Fig. 1. Scheme of the experimental procedure in this study.

corresponds to the number of 90 to 110 individual fibres, regardless of the type, was placed between the graphite elements and heated to a set temperature of 1100 °C. Methane as a carbonous gas was introduced into the reactor at a flow rate of 2 l/h, diluted with nitrogen at a flow rate of 10 l/h, for 120 s. In the next phase, the sample was stored in an inert atmosphere without CH4 flow at the synthesis temperature for another 60 s. During the synthesis process, the maximum supplied current was 2.4 A. Thereafter, CF/PyC composite samples were obtained: S/PyC 1100 °C and G/PyC 1100 °C with 54.2 ± 6.5 % and 53.0 ± 5.0 % of pyrolytic carbon as a matrix, respectively.

The samples obtained at 1100 °C were divided into three parts. The first part of the samples, i.e. samples S/PyC1100 °C and G/PyC1100 °C were already subjected to direct further study, and the other two groups were subjected to additional heat treatment in accordance with Fig. 1. The second part of the samples was subjected to an additional heat treatment temperature of 1600 °C, obtaining S/PyC1600 °C and G/PyC1600 °C samples. The third was heated and maintained at 2000 °C, obtaining S/PyC2000 °C and G/PyC2000 °C samples. For this thermal treatment, a high-temperature flow tube furnace for graphitization with water cooling was used. In each case, the thermal processing to these temperatures was carried out in a protective atmosphere of argon, with a heating rate of 10 K/min to the set temperature, holding at this temperature for 10 min and free cooling.

2.3. Methods

2.3.1. Morphology and microstructure

The microstructure and morphology of carbon fibres and CF/PyC composites were evaluated using the Nova NanoSEM 200 scanning electron microscope (FEI Europe Company) and the Thermo Fisher Scientific SCIOS II Dual Beam scanning electron microscope (SEM). The SEM images were also used to evaluate the diameter of the carbon fibres in the composites using ImageJ v1.53e software. In total, 50 fibres were measured for each type of sample.

A digital microscope (VHX—900F) was also used to analyse the average diameter of CF/PyC composites and the surface morphology of the samples. It was equipped with a standard lens and a Z500T lens, capable of working with resolutions from 20× to 200×. The working distance was 4.4 mm. Similarly, digital images were used to measure the diameters of the CF/PyC composites produced using ImageJ v1.53e software. A total of 300 measurements were conducted for each type of sample.

The microstructure characterisation was performed with a transmission electron microscope (TEM) using Thermo Fisher Scientific Titan Themis Cs corrected to 200 kV xFEG. Thin films for TEM observations were cut using the Focused Ion Beam (FIB) technique employing Thermo Fisher Scientific SCIOS II Dual Beam SEM.

2.3.2. Structure

Using also images from TEM and High-Resolution Transmission Electron Microscope (HRTEM), the structure of the materials was determined. DigitalMicrograph 3, also known as Gatan Microscopy Suite 3, was used for quantitative evaluation based on TEM images.

To carry out X-ray diffraction analyses using the X-ray Diffraction (XRD) technique, a Panalytical X'Pert Pro X-ray spectrometer (PANalytical, Malvern, UK), equipped with a Cu K-type X-ray source (λ = 0.15406 nm), was used. The procedure for recording diffractograms was carried out with an angular increment of 0.02° in the 2θ angle region from 5 to 90°. The obtained diffraction patterns were analysed in detail using Fityk software version 0.9.8 [41]. To determine the interplanar spacing (d_{002}), the Bragg eq. (Eq. (1)) was used, the average size of graphite domains along the c-axis (L_c) the Scherrer eq. (Eq. (2)), and the determination of the number of polyarene layers in the packet (N) based on Eq. (3). Parameters were determined using G(002) reflectance analysis. In turn, to calculate the average size of graphite domains along the a-axis (L_a), Eq. (4) was used based on G(100) reflection analysis [42,43].

$$n\lambda = 2 \cdot d_{002} \cdot sin(\theta) \tag{1}$$

$$L_c = \frac{K \cdot \lambda}{\beta_{002} \cdot coscos\ (\theta)} \tag{2}$$

$$N = \frac{L_c}{d_{002} + 1} \tag{3}$$

$$L_a = \frac{K \cdot \lambda}{\beta_{100}(\theta)} \tag{4}$$

where n is the diffraction order (1), λ represents the wavelength of the radiation, d is a measure of the distance between graphene planes, K is the aspect ratio (taken to be about 0.94), β expresses the width of the diffraction peak at half its maximum height, while θ is the Bragg angle.

The Raman spectroscopy was carried out using a WITec Alpha 300 M + camera with an 1800 g/mm grating, a 532 nm diode laser and a 50× objective. A total of ten accumulations with 20-second integration times were recorded for each line measurement point. The scans were taken to a depth of 4 μm at 0.5 μm intervals. Deconvolution of the spectra was performed with the Voigt function [44] using Fityk 0.9.8 software. With this, the characteristic bands corresponding to the vibration of the carbon structures in the samples were determined. The I_D/I_G and I_{2D}/I_G ratios were determined using the total area of the D and G and 2D and G

bands, respectively, as coefficients describing the degree of crystallinity of the carbons. Similarly, $I_D/I_{D'}$ was determined from the surface areas of the D and D′ bands and the degree of defectivity of their graphene planes. In addition, using the Cançado eq. (Eq. (5)) [45], the average size of L_a crystallites was determined from the three spectra for each sample:

$$L_a = (2,4 \cdot 10^{-10}) \cdot \lambda^4 \cdot \left(\frac{I_D}{I_G}\right)^{-1} \quad (5)$$

where L_a is a crystallite size, λ is the radiation wavelength [nm] and I_D/I_G are the intensity of Raman D and G bands.

2.3.3. Texture

Diffraction images obtained using the SAED method made it possible to measure the level of preferred orientation of carbon domains in pyrolytic carbon, referred to as the orientation angle (OA). The process began by determining the location of the centre of the diffraction ring pattern and the length of the radius of the diffraction circle with indices (002). Then, using a specially prepared script in Python, changes in light intensity were measured around the perimeter of a circle with a predefined centre and radius, recording values every 0.33°. Based on this profile, two Gaussian curves were fitted, which reached their maximum values at the brightest points on opposite sides of the circle. The half-width FWHM of these curves was measured, and their average value was defined as OA. For each type of sample, 30 measurements were taken to determine OA, for a total amount of 180.

2.3.4. Ultrasonic dynamic measurements of Young's modulus

Ultrasonic dynamic measurements of Young's modulus were carried out using the through-transmission method of longitudinal ultrasonic waves (two heads: transmitter and receiver). A materials tester "materials tester CT3" from Unipan-Ultrasonic Poland was used. The settings of the apparatus during the measurement were: energy: 600 V, repetition rate: 1 Hz, gain +20 dB, head frequency f = 1 MHz at 20 mm diameter.

Measurements for carbon fibres were made by fixing the fibre bundle in the centre of the heads, and then the fibres were stretched to the maximum and the ultrasonic wave propagation time was read. The fibre bundle was then shortened, and the ultrasonic wave propagation time was measured again for the new beam length. The procedure was repeated by further shortening the fibres.

CF/PyC composites were measured by closely placing composite rods of a fixed length between the centres of the heads and reading the ultrasonic wave propagation time.

Eq. (6) relating to a one-dimensional medium was used to calculate the dynamic Young's modulus [46]:

$$E = \rho \cdot V_L^2 \quad (6)$$

in which: E - Young's modulus [GPa], ρ - apparent density of the sample [g/cm3], V_L^2 - velocity of the longitudinal ultrasonic wave [m/s].

3. Results and discussion

3.1. Morphology and microstructure of CF/PyC composites

Within the scope of this investigation, a detailed morphological and microstructural analysis of all fabricated carbon/carbon (C/C) composites was conducted utilising both digital microscopy (Fig. 2) and scanning electron microscopy (Fig. 3), following both the synthesis process and a subsequent heating stage.

The results of the surface morphology analysis demonstrated significant consistency across different experimental procedures. The observed pyrolytic carbon layers were characterised by smoothness and a subtle lustre, indicative of this material type, supplemented by the sporadic presence of randomly distributed ball-like protuberances (Fig. 2b) [47]. Furthermore, the orientation of the composite bundle core indicated an axis around which successive PyC layers were concentrically deposited, resulting in a thickening of the core's geometry, and reflecting the fibrous nature of the substrate, thereby ensuring a uniform coverage over the entire filament.

The measurements of composite diameters, presented in Fig. 4a and b, confirmed this. The observed changes in diameters for the final temperatures of thermal treatment of composites, which were 1100, 1160, and 2000 °C, reached values of 248 ± 29, 248 ± 42, and 243 ± 30 μm for S/PyC (Fig. 2a, c, e) and 255 ± 46, 234 ± 36, and 232 ± 41 μm for G/PyC (Fig. 2b, d, f), respectively. It is postulated that the relatively large standard deviation values can be attributed to the lack of a perfectly circular cross-sectional shape of the samples, which is a direct consequence of the specific methodology for obtaining composites. The ends of carbon fibres (CFs) were placed between graphite spacers, clamped, and gently flattened, which, after stretching the bundle along the axis, gave them a preferential orientation. The circular-oval shape of the cross-section was further confirmed by SEM images (Fig. 3g-m). The analysis of histogram data (Fig. 4b) suggests a subtle shift in the distribution towards lower diameter ranges.

A similar situation occurred for the measurements of CF diameters from SEM cross-section images. The main range of diameter changes coincides with the standard deviation of the sample, and the results are presented in Fig. 4c. In the case of CF-S fibres, a certain tendency to reduce the fibre diameter with an increase in the thermal treatment temperature can be observed, which may result from structural changes and the accompanying rearrangements inside the low-modulus carbon fibre [48]. To confirm the changes occurring inside the fibres, it is necessary to carry out a structural and surface analysis of the tested fibres as a result of thermal treatment at temperatures of 1600 °C and 2000 °C [48].

Porosity was considered on equivalent and analogous samples in our previous article [19]. The synthesis method produced CF/PyC samples with negligible porosity, as evidenced by the relatively small interfiber spaces. This had the favourable effect of filling the void spaces within the matrix and highly densifying the core, as was the case here. In the C/C composites obtained in this study, the adhesion and contact between

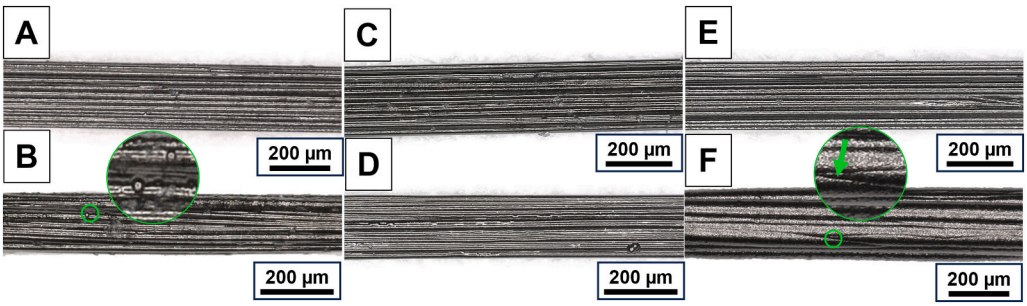

Fig. 2. Digital microphotographs of morphology of the obtained PyC-coated composites CF-based: CF-G (a, c, e) and CF-S (b, d, f) before (a, b) and after additional heat treatment at 1600 °C (c, d) and 2000 °C (e, f), respectively. The arrow (f) points to the micro-crack.

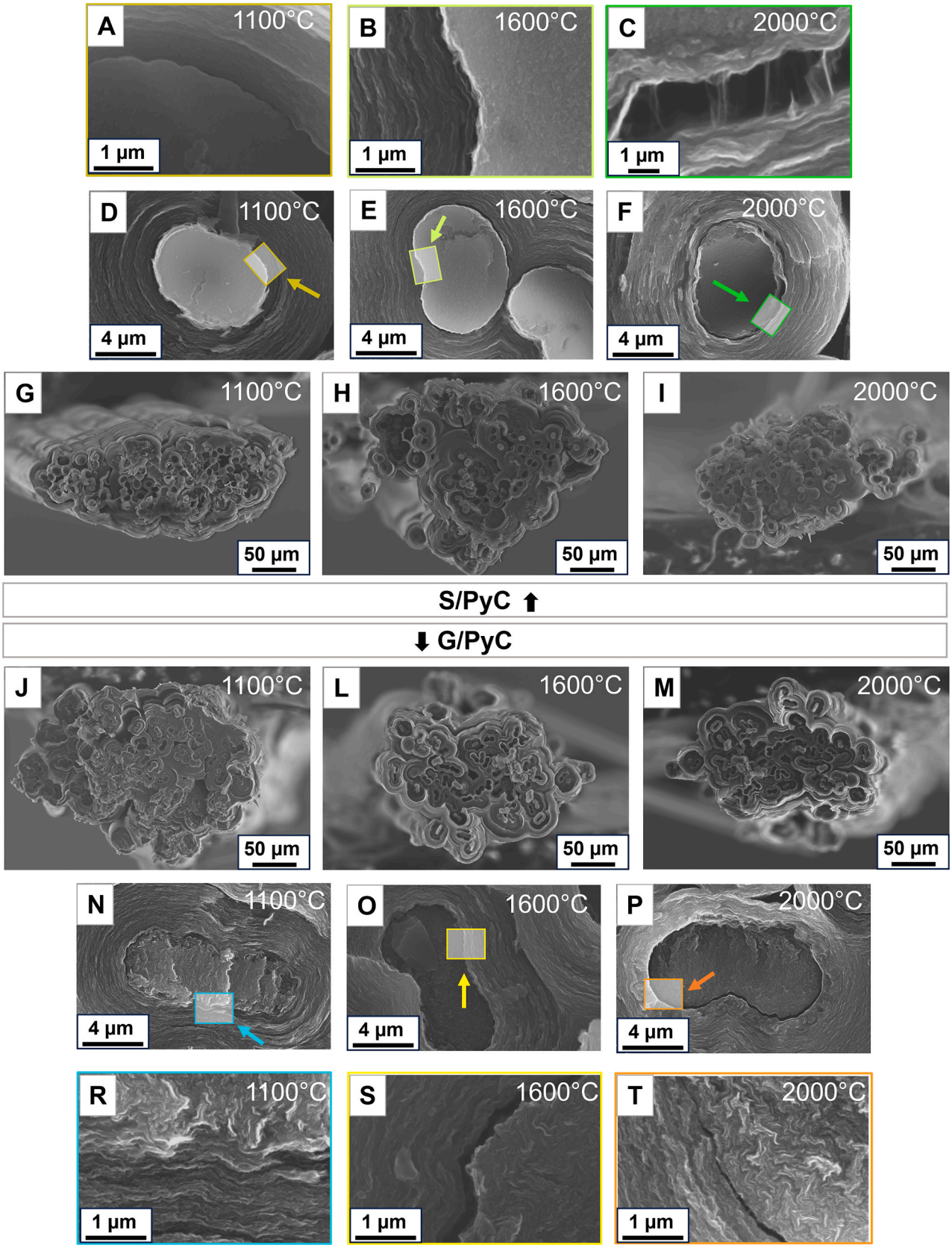

Fig. 3. SEM analysis of cross-sections of the obtained composites (a-t) depending on the temperature treatment. These are samples of: S/PyC X (a-i) and G/PyC X (j-t) where X is the temperature shown on the image. The arrows, along with the highlighted areas in the images (d-f, n-p), indicate the areas of the continuity (d,n) and discontinuity (e-f, o-p) interfacial boundaries or PyC laminar layers around the boundary. This is illustrated respectively by the magnifications shown at (a-c, r-t).

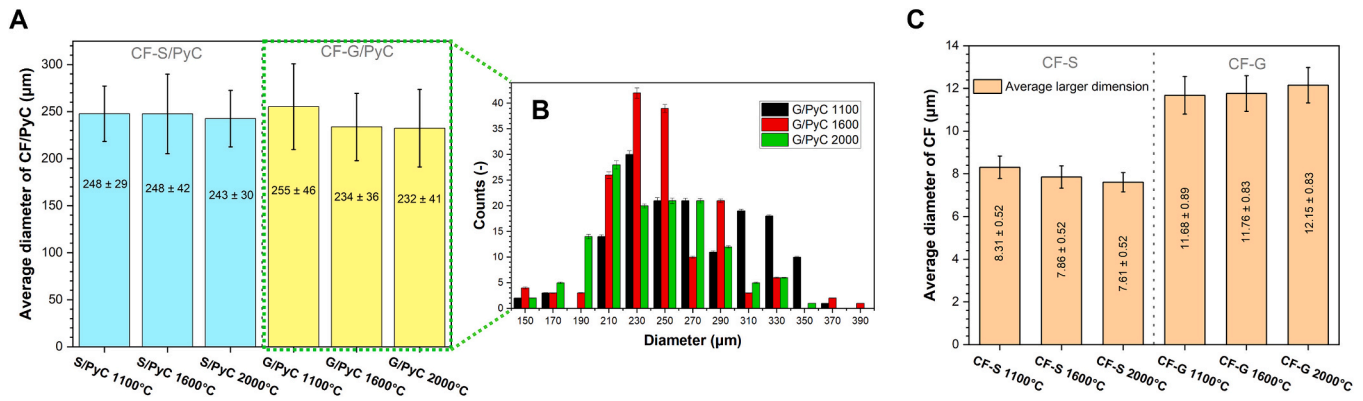

Fig. 4. Graphs of the average diameter of the composite (a) with a histogram plotted to G/PyC (b) and the long cross-sectional dimension (equivalent to its diameter) of the carbon fibres (c) as a function of final temperature.

the matrix and the fibre were generally strong, ensuring the interphase continuity of the composite at the microstructural level, showing a close adhesion of PyC to the core fibres after CVD synthesis, and forming concentric, laminar layers. Thermal processes played a critical role in maintaining the integrity of these phases, and the matrix-fibre interface was characterised as a function of thermal treatment. Despite the overall continuity, delamination was observed in some areas of the composite. Observations of cross sections of S/PyC (Fig. 3a-i) and G/PyC (Fig. 3j-t) composites showed discontinuities at the interface or in adjacent PyC layers, with a tendency for these defects to become more visible with increasing temperature of heat treatment. At the maximum treatment temperature, single defects were also observed in digital microscopy images. For the S/PyC 2000 °C sample, microcracks were observed at the boundary with the twisted core fibre (Fig. 2f-arrow). Such a phenomenon can be attributed to the probable evolution of pores trapped in the composite voids and the shrinkage of some CF fibres, as seen above, leading to microcracks in micro-regions parallel and perpendicular to the axis.

The mechanical strength of carbon composites significantly depends on the load distribution between fibre and matrix, with insufficient adhesion weakening the composite, while excessive bonding may cause brittle fracturing [45,49]. It was also noted that the higher the final treatment temperature, the more likely that the interface between phases could degrade (Fig. 4a-c, r-t), likely due to local thermal stresses and the shrinkage of CFs [50].

3.2. Structure and texture of CF/PyC composites

3.2.1. XRD

The general characterisation of the phase composition and crystallographic structure of the heated CFs and obtained composites was studied by XRD.

The diffractograms for CF-S and CF-G (Fig. 5a) showed reflections in the region of the 26° angle 2θ, similar to the reflections obtained for the composite samples (Fig. 5b), which originate mainly from the PyC matrix and partly from CF reflections This is noticeable especially for CF-S-based S/PyC composites. This position is typical of G(002) graphene plane reflections [43]. The diffractograms of CF-G fibres exhibit a sharp and intense G(002) peak, as well as a visible G(004) peak, in contrast to the diffractograms of CF-S samples. Furthermore, G(100) reflections around 43° were observed in all spectra. It is worth noting that the G (002) peak for all CF-S samples has a significantly lower intensity and a larger half-width, which suggests a more amorphous nature of the graphene planes in their structure. As the temperature for heat treatment

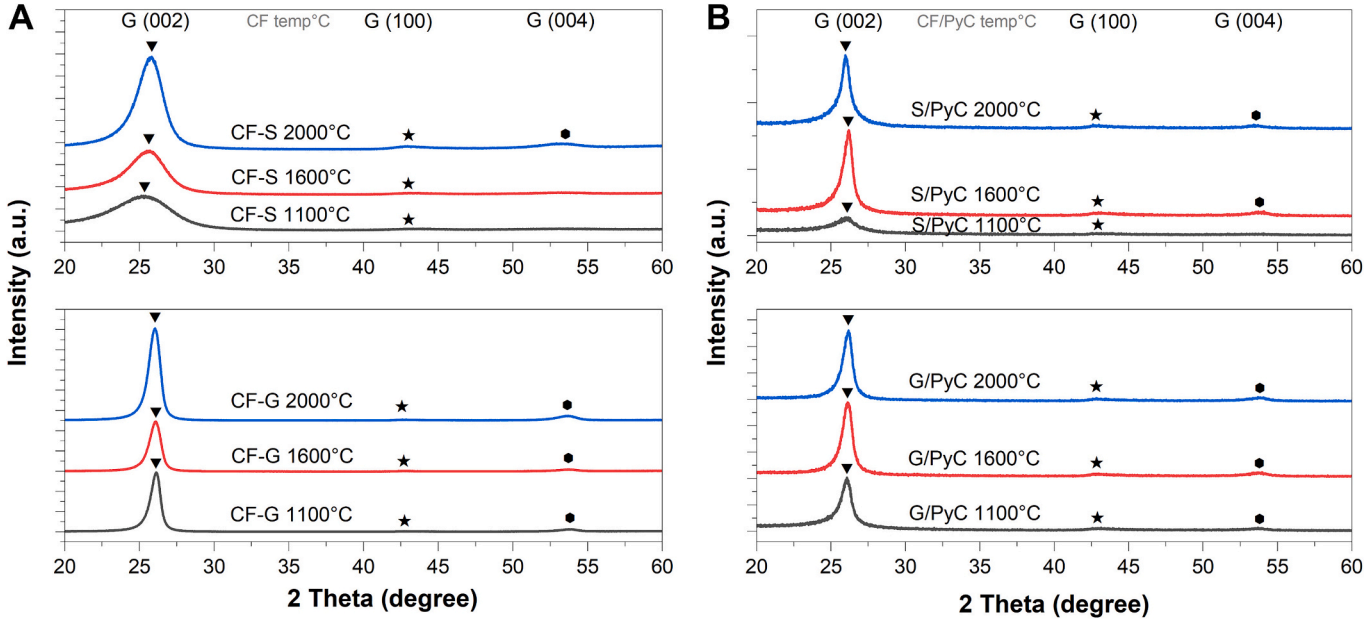

Fig. 5. XRD diffractograms for carbon fibres (a) and CF/PyC composite (b) samples.

increases, the peak position shifts towards larger values of 2θ angle for CF-S. At 1100, 1600, and 2000 °C, the position is 25.32, 25.44, and 25.71°, respectively. This shift results in a noticeable decrease in the interplanar spacing d_{002} (Table 2) and domain ordering. Additionally, the increase in crystallinity is accompanied by an average doubling of crystallite dimensions within both the (002) L_c and (100) L_a planes (Table 2). This is also confirmed by the N-number of polyarene layers in the packet.

The parameters for CF-S2000 °C, which direct the structure of the fibre to the turbostratic carbon, have smaller values than those determined for CF-G1100 °C. It is worth noting that, regardless of the treatment temperature, the position of the G (002) peak for CF-G was 26.06°. According to Table 2, there was no significant increase in crystallinity and ordering as the temperature increased, only a negligible increase in crystallites. When examining the structures of CF-S and CF-G carbon fibres, it becomes apparent that the temperature at which the fibres are obtained has a notable impact on their structure, even after undergoing further thermal treatment. In the case of CF-G fibres, which are commercially obtained at temperatures above 2000 °C, the impact of thermal treatment at 1100, 1600 and 2000 °C on structural changes is negligible. In the case of CF-S, it may be advisable to consider additional heat treatment at 1600 and 2000 °C. This process promotes a rearrangement of the carbon structure from amorphous to turbostratic, resulting in a visible decrease in the average diameter of CF-S. These observations demonstrate significant differences in structure and properties between the fibre types used (Table 2).

The diffractogram from S/PyC1100 °C exhibits a lower intensity of the G(002) reflectance (Fig. 5b), indicating the more amorphous character of the composite [51]. The diffractogram is therefore the result of diffraction from the more amorphous CF phase and the less amorphous matrix phase, PyC. As the processing temperature of the composites increases, the peak position shifts towards larger values of 2θ angle for G/PyC. The values measured were 26.06, 26.12, and 26.16° for 1100, 1600, and 2000 °C, respectively. This led to a decrease in the interplanar spacing d_{002} and a subtle observable ordering of the domains with some growth for both phases (Lc, N, La) as a function of temperature (Table 2). The S/PyC composite exhibited a minor change in interplanar spacings, with the smallest value obtained at 1600 °C for a G(002) peak of 26.13°. This parameter slightly decreased to 26.03° at the highest temperature of 2000 °C and returned to a value close to the initial 25.99° at 1100 °C. This non-uniformity is related to the elementary structure of pyrolytic carbon, whose deposition cannot be perfectly predicted and modelled [52], and the structure of the fibre used. It is recommended that a localised analysis of the PyC system be conducted to identify which areas undergo structural changes because of temperature fluctuations and which ones remain stable. As shown in Table 2, the average crystallite sizes (L_c) in the c-axis direction (002), the number of planes (002) in the packets, and their lengths (L_a) in the a-axis direction (100) for both types of composites exhibit a gradual increase. These findings corroborate the hypothesis that the heat-treatment temperature decisively influences both the structural evolution and the domain expansion within the PyC matrix [53]. Reflections from other planes of the crystallographic lattice G (100) at approx. 43° and G (004) at approx. 54°, which are more intense the higher the temperature of action, may testify to the turbostratic nature of the produced PyC composite with a tendency towards graphitization.

3.2.2. HRTEM and SAED

High-resolution transmission electron microscopy (HRTEM) was utilised to quantify the dimensions of the crystallites along the c-axis. Selected area diffraction patterns (SADPs) were employed to determine interplanar d_{002} spacings, texture, and orientation. The analysis aimed to investigate the effect of temperatures up to 2000 °C on local structural changes in the composite area.

Figs. 6 and 7 illustrate the structure and texture of the synthesised PyC on CF-S (left) and CF-G (right) at 1100 °C (Fig. 6a, b), and after additional heat treatment at 1600 (Fig. 6c, d) or 2000 °C (Fig. 6e, f). Figs. 7 and 8 display PyC types treated at 2000 °C. The structural response of CFs to temperature changes was assessed using HRTEM images presented in the supplementary section (Fig. S1). That was also a confirmation of structural differences in CFs derived from, among others, the XRD study. Diffractograms were generated for each region, displaying three characteristic rings originating from graphite planes (002), (100), and (110) with scattering vectors of 2.8, 4.8, and 8.2 nm^{-1}, respectively. The diffraction images of the CFs indicated a directional intensity distribution associated with the (002) planes, indicating an anisotropic orientation of the crystalline domains, in contrast to the PyC diffraction.

Additionally, the orientation angle measure (OA) revealed the existence of two types of pyrolytic carbon. Table 3 presents the statistical results obtained from a nano-area of approximately 10 nm using a scattering vector of 2.8 nm^{-1}, while Fig. 7 provides a graphical representation. It is worth noting that the areas where low-textural (LT) PyC (Fig. 7a, b, h, j) and medium-textural (MT) PyC (Fig. 8c, d, e, i) coexist did not show any changes under additional treatment. LT PyC is also known as dark laminar (DL) and is sometimes categorised as isotropic PyC, while MT PyC is referred to as smooth laminar (SL) [54]. The values for S/PyC remain practically unchanged, and for G/PyC, all differences coincide with the standard deviation from the measurement samples. Analysis of the interplanar spacings d_{002} (Table 3) from HRTEM images of the matrix, identified similar ordering of PyCs at analogous temperatures. This confirmed a more turbostratic PyC structure than the XRD study for S/PyC samples, for which the signal was the result of CF and PyC diffraction.

The appearance of different types of PyC may indicate a mixed mechanism for PyC growth [19,37]. The examples of heterogeneity of the sample matrices are depicted in Fig. 8. The occurrence of different areas of structural order in the pyrolytic carbon in the S/PyC composite heat treated at 2000 °C is explained by the examples shown in Fig. 9.

While the literature does not directly discuss the specific effect on the reorientation of pyrolytic carbon domains, it is possible that a temperature of 2000 °C may not be sufficient to induce the desired changes in orientation and texture, suggesting only an insignificant effect on the coefficient of thermal expansion and preferred orientation [55]. Further research is needed to fully understand the kinetic and thermodynamic factors affecting these properties.

Table 2
Structural parameters (d_{002}, L_c, N, L_a) determined XRD methods for CF and CF/PyC of composites.

Sample	Parameters	d_{hkl} [nm]		L_c [nm]		N [−]		L_a [nm]	
Type of CF	Temp. of heat-treatment	CF G(002)	CF/PyC G(002)	CF G(002)	CF/PyC G(002)	CF G(002)	CF/PyC G(002)	CF G(100)	CF/PyC G(100)
CF-G	1100 °C	0.342	0.342	7.73	10.91	24	33	7.16	5.52
	1600 °C	0.342	0.341	8.61	12.18	26	37	7.26	5.66
	2000 °C	0.342	0.340	8.74	12.99	27	39	7.75	6.37
CF-S	1100 °C	0.351	0.343	1.92	4.23	6	13	2.56	3.68
	1600 °C	0.350	0.341	2.75	10.15	9	31	3.40	5.52
	2000 °C	0.346	0.342	3.88	10.32	12	31	5.08	5.53

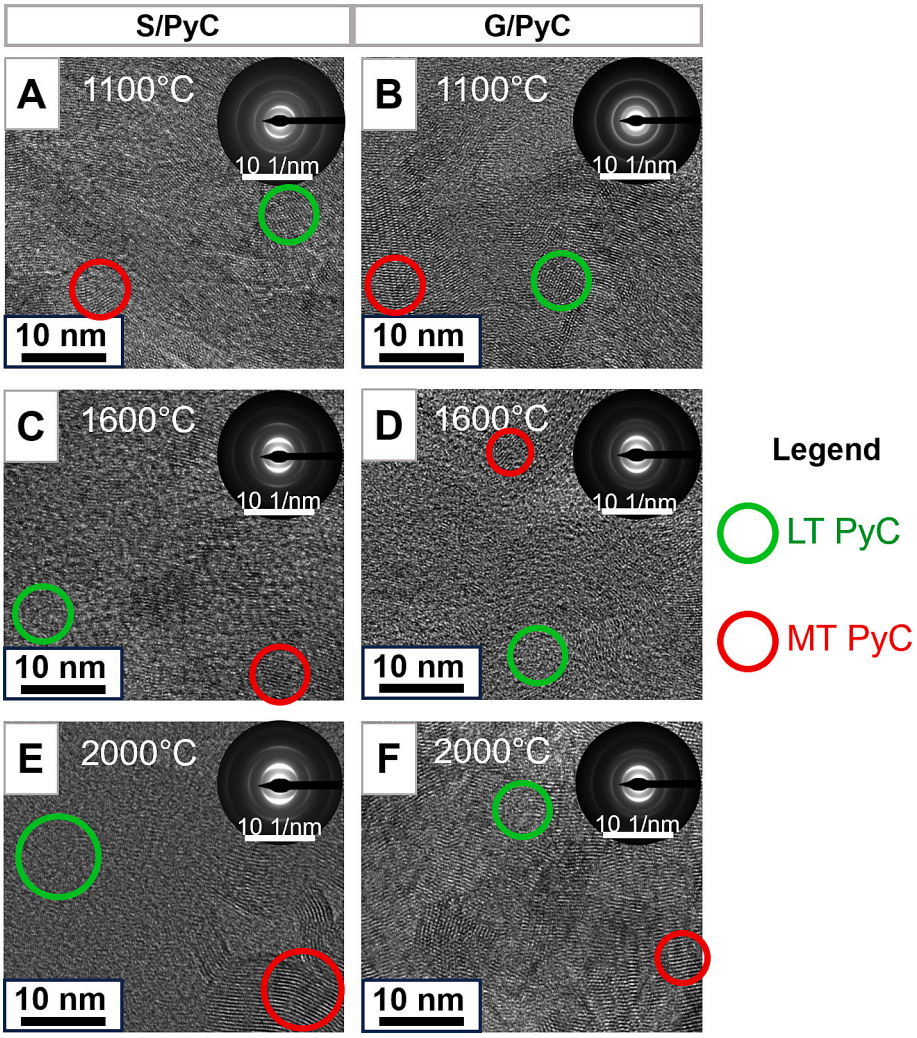

Fig. 6. HRTEM images with SAEDs taken independently of matrix into S/PyC (a, c, e) and G/PyC (b, d, f) samples heated to 1100 (a, b), or 1600 (c, d), or 2000 (e, f) respectively.

3.2.3. Raman spectroscopy

Raman spectroscopy was utilised to analyse the structure of C/C composites and to assess their characteristics in comparison to PyC with CF, which are the main components of the composite. Fig. 9 shows Raman spectra for: (a) carbon fibres (CFs) subjected to specified heating temperatures, with (c) a detailed decomposition into first-order bands (1750–1000 cm^{-1}) illustrated for a CF-S sample at 1100 °C. Panel (b) presents the Raman spectra of composites, while (d) charts the graphitization trajectory, integrating data points for G peak positions (ω) and the R1 parameter, representing the ID/IG ratio across varying temperatures. The analysis employed a five-band model, encapsulating: the G band (~1580 cm^{-1}), attributed to E_{2g} stretching of sp2 C=C bonds; the D resonance band (~1360 cm^{-1}), linked to transient defects within the graphite structure; the D′ band (~1620 cm^{-1}), sensitive to defect types; and the D4 (~1200 cm^{-1}) and D3 (~1500 cm^{-1}) bands, both associated with hydroxylated and disordered carbon forms. Additionally, the spectrum's extended range incorporates the 2D, D + G, and 2G bands, signifying the overtones of primary bands [56,57]. This comprehensive spectral decomposition reveals the intricate relationship between structural disorders and the graphitization ability, underscoring Raman spectroscopy's critical capability to trace the structural evolution of carbonaceous materials under thermal influence.

Based on the areas under the Raman spectra curves, the ratio of integrated intensities of the D and G bands, commonly regarded as the R1 index of structural ordering, was calculated. This index is instrumental in assessing the crystallisation and amorphisation trajectories of graphitic materials [58]. The data are presented relative to the heating temperatures, namely 1100, 1600, and 2000 °C. Carbon fibres (CF-G) do not exhibit significant shifts in the G band position, oscillating around 1581 cm^{-1}, specifically: 1581.6 ± 1.2, 1580.6 ± 0.2, and 1581.5 ± 0.4 cm^{-1}, corresponding to R1 values of 0.61 ± 0.15, 0.60 ± 0.20, and 0.51 ± 0.05, respectively. The graphitisation trajectory chart (Fig. 9d) indicates a subtle shift towards structural ordering of graphite, corroborated by the measured crystallite sizes (L_a). This parameter increased from 31.71 ± 8.17 to 37.93 ± 3.59 nm, respectively for temperatures of 1100 and 2000 °C. However, domains in the fibre at 1100 °C are already well-formed. Thus, no significant change was noticed. A stronger predisposition for rearrangement from amorphous to turbostratic structures is demonstrated by the second type of fibre, produced at temperatures below 2000 °C. As shown in the chart, the shift in the G band position for CF-S is significant, changing from 1593.5 ± 2.1, through 1594.0 ± 1.3 to 1583.6 ± 0.3 cm^{-1}. Correspondingly, the R1 parameter for these fibres was: 2.15 ± 0.30, 1.42 ± 0.15, and 1.11 ± 0.08. Such a decline unequivocally indicates a reduction in defect concentration in favour of domain growth. Moreover, with increasing storage temperature, distinct second-order bands emerge, leading to an increase in the R2 parameter, confirming this relationship. R2 values are provided in the supplement (Table S1). At 2000 °C, fibres still differ structurally from each other. Comparing the R1 parameter, it was observed that CF-G possesses a more ordered and developed structure, as well as larger crystallite sizes.

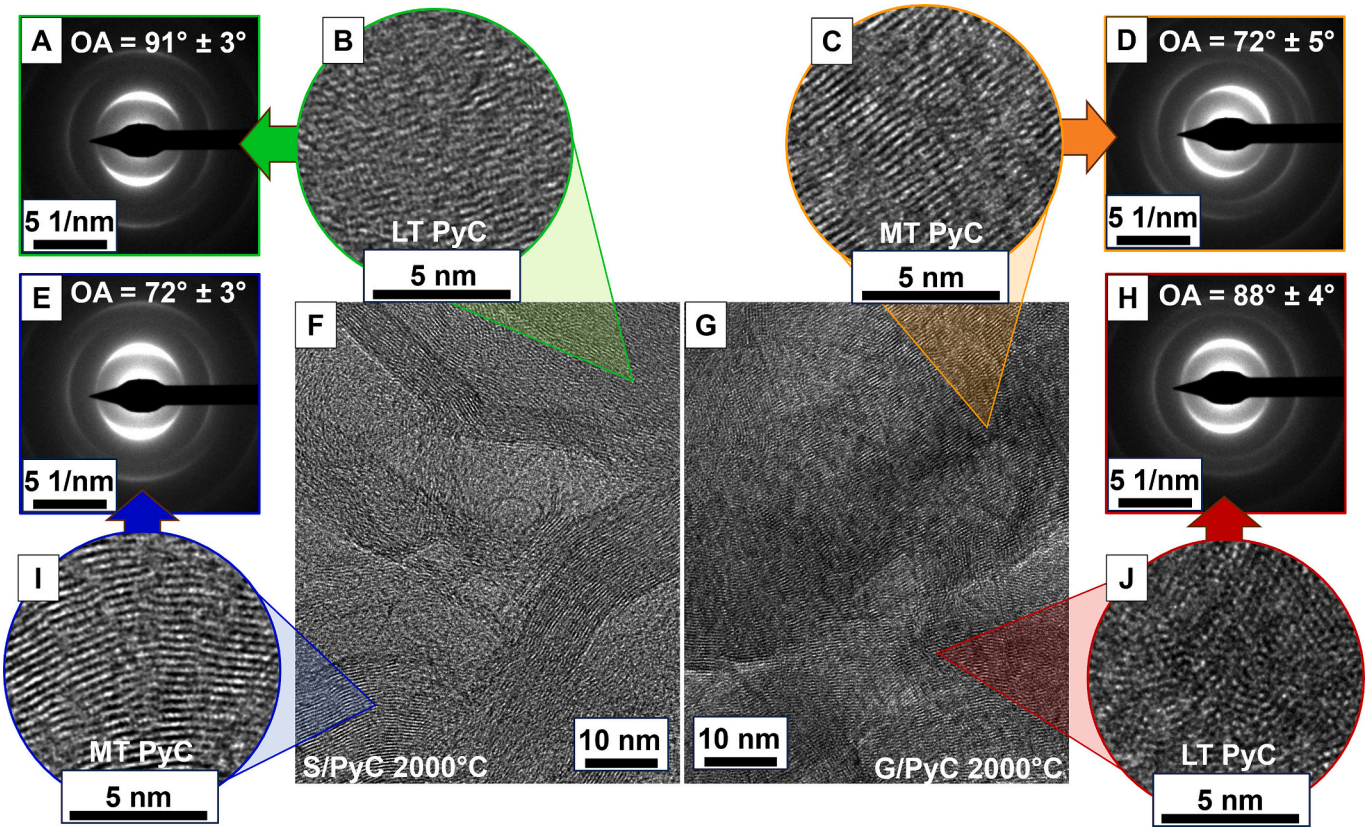

Fig. 7. HRTEM images of PyC of S/PyC 2000 °C (b, f, i) and G/PyC 2000 °C (c, g, j) samples, and SAEDs taken independently of HRTEM from two regions of PyC (a, d, e, h).

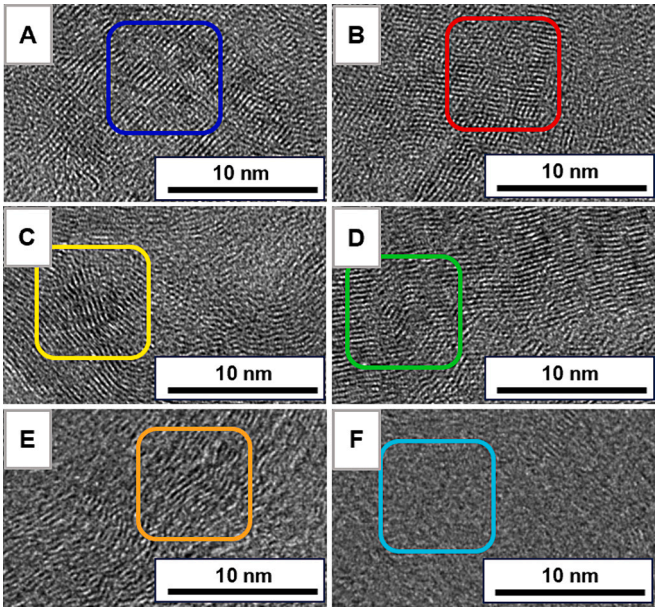

Fig. 8. Texture differences based on the example of S/PyC 2000 °C sample: (a, d) rapid, irregular disruptions in packet continuity, culminating in an expansion of interplanar spacings; a pronounced divergence in orientation along (b) directions perpendicular and parallel to the a-axis, and (c) parallel to the c-axis; alongside (e) the irregular development of domains, and (f) the amorphous nature of the carbon phase.

Table 3
List of the orientation angle values (OA) for low- and medium-textured (LT and MT) and the interplanar spacing of PyC for each type of C/C composite.

Parameter	OA [°] of PyC		d_{002} [nm]
Sample	LT (DL)	MT (SL)	PyC (HRTEM)
G/PyC 1100 °C	91 ± 5	71 ± 4	0.342 ± 0.004
G/PyC 1600 °C	91 ± 5	72 ± 4	0.341 ± 0.004
G/PyC 2000 °C	88 ± 4	72 ± 5	0.339 ± 0.003
S/PyC 1100 °C	90 ± 4	72 ± 3	0.342 ± 0.003
S/PyC 1600 °C	91 ± 3	72 ± 4	0.340 ± 0.002
S/PyC 2000 °C	91 ± 3	72 ± 3	0.339 ± 0.001

For S/PyC 2000 °C, the La parameter was 17.30 ± 1.25 nm, and L_a was only half of that for G/PyC 2000 °C.

For PyC, irrespective of the substrate, a similar graphitisation trajectory and crystallite size growth were obtained. These are shown in the HRTEM images (Figs. 6, 7, 8). Both LT and MT PyC fall within the domain growth area of graphite crystallites, subject to a reduction in sp3 bond content [58]. The G band shift for G/PyC was from 1589.2 ± 0.9 through to 1583.7 ± 0.5 cm^{-1}, and for S/PyC from 1588.9 ± 0.3 to 1582.8 ± 0.1. The change in integrated ID/IG intensity is also similar for both types of samples. The change in heating temperature influenced this parameter to shift from 1.29 ± 0.06, through 1.18 ± 0.08, finally decreasing to 0.77 ± 0.04 for G/PyC. For S/PyC, it fell from 1.25 ± 0.14, through 1.13 ± 0.07 to 0.73 ± 0.01.

A general tendency of PyC structure changes towards graphitisation was shown, according to its trajectory (Fig. 9d). Possible imbalances and inhomogeneities in PyC, probably resulting from the non-uniform process of methane pyrolysis on the fibre. These are attributed to the synthesis process, which is potentially affected by the concentration and ratio of PAHs to C_2 particles [59–61], thus affecting the formation of a

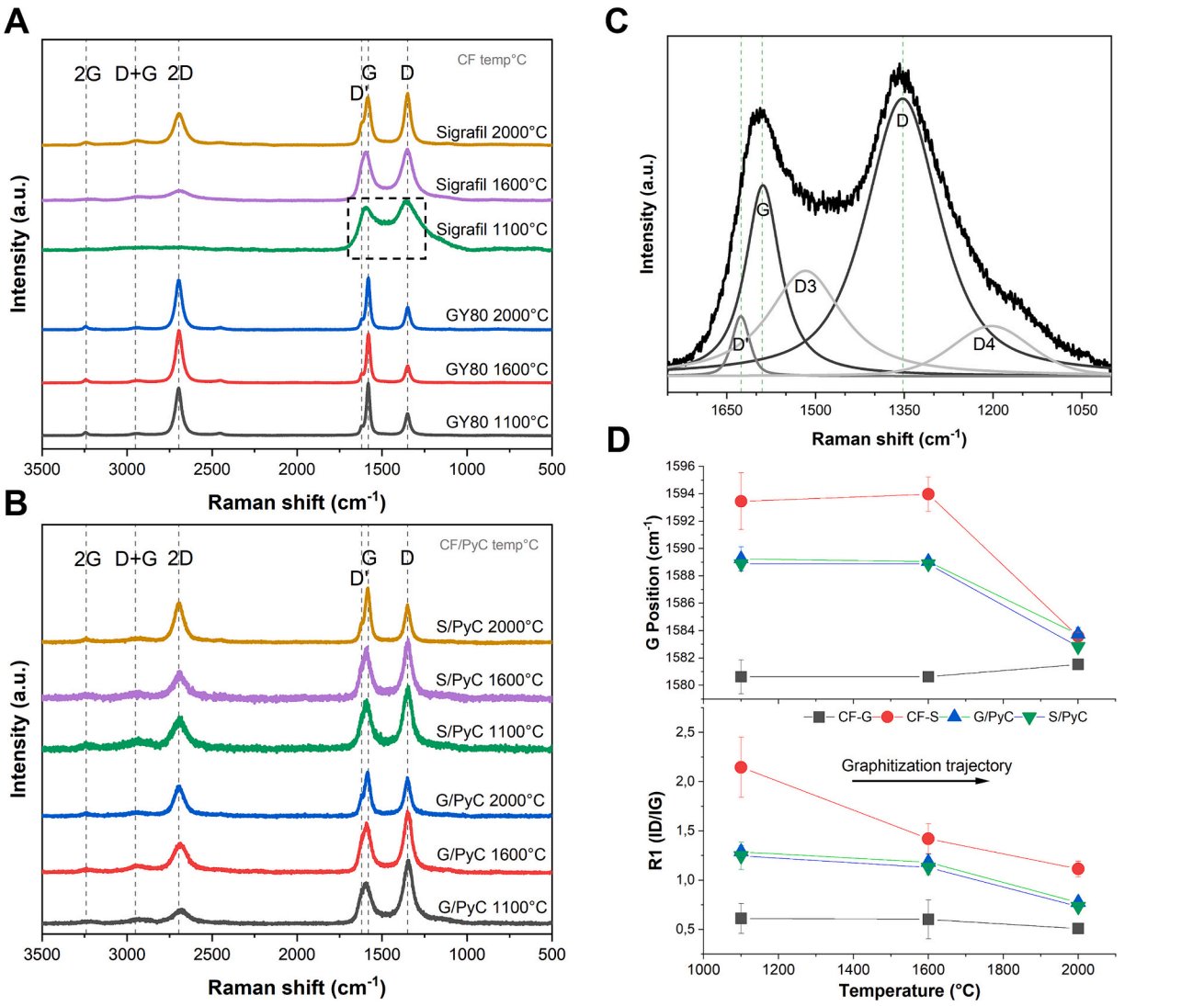

Fig. 9. Raman spectra for samples differing in heating temperature: (a) CF and (b) PyC from composites. Panel (c) shows first order Raman spectrum of amorphous CF-S 1100 °C and (d) graphitization of these samples.

defect-rich structure of PyC's. It is believed, therefore, that a temperature of 1600 °C should promote the thermodynamic initiation of ordering processes, albeit limited by kinetics. The temperature of 2000 °C was sufficient to reduce the level of structural defects in favour of the development of bands indicative of graphite crystallisation in the produced PyC, which causes the most significant growth of crystallites. Initially, for a temperature of 1100 °C, the L_a parameter was 14.95 ± 0.7 and 15.51 ± 1.72 nm for PyC crystallites from G/PyC and S/PyC samples, respectively. As the temperature increased, these values gently increased to 16.30 ± 1.15 and 17.04 ± 1.12 nm at 1600 °C, until for 2000 °C the average dimensions of the crystallites in the direction increased significantly to 24.86 ± 1.32 and 26.16 ± 0.16 nm. This confirms the previously suggested trend of growth of graphitic domains within PyC based on XRD studies.

3.3. *Stiffness properties on the example of dynamic Young's modulus*

Ultrasonic dynamic measurements of Young's modulus were carried out using the through-transmission method of longitudinal ultrasonic waves for composites obtained at a temperature of 1100 °C and after heat treatment at 1600 °C and 2000 °C. The highest value of Young's modulus was observed for samples obtained at 1100 °C, namely at the temperature of PyC synthesis (Fig. 10).

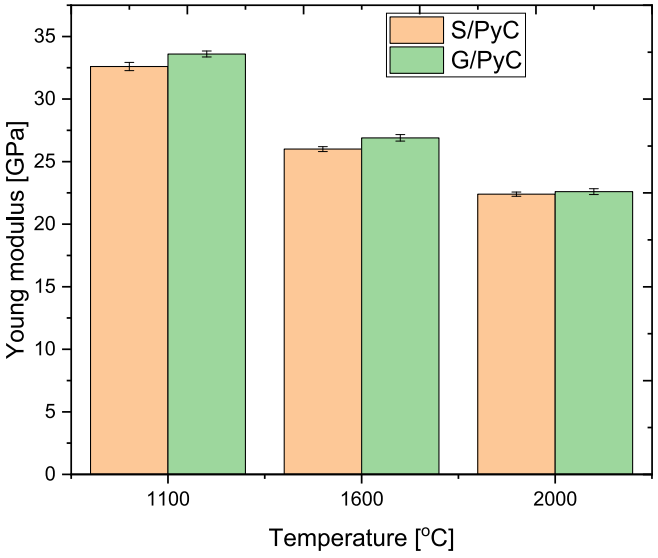

Fig. 10. Young modulus of composites as a function of heat treatment temperature.

These values for both the composite with low- and high-modulus fibres were comparable and amounted to approximately 33 GPa. These values are relatively low considering the Young's modulus of the fibres provided by the producers. For this reason, the Young's modulus of both kinds of carbon fibre were also measured using the ultrasonic method. These values were 114.2 ± 4.77 GPa and 87.9 ± 8.25 GPa for CF-G and CF-S fibres, respectively, and therefore much below the values declared by the producers. These differences are due to different measurement methods, namely static tensile testing in the case of the manufacturer's data and the ultrasonic method in the case of the tested samples. In the case of the static method, the result reflects the value of relaxed Young's modulus (relaxation time of the order of 10^{-3} s), while in the case of the ultrasonic method, the result is the unrelaxed Young's modulus (relaxation time of the order of 10^{-6} s).

Moreover, considering observations during measurements and our own experience, the authors state that the highest values of the determined ultrasonic wave transit time as well as Young's modulus are the lower limit for the tested fibres. This is related to the issue of fibre adhesion to the head and fibre tension during the test. However, when comparing the results of the Young's modulus of fibres made using the ultrasonic method with the results for composites, we also observe a reduction in properties. This is related to the properties of the matrix itself, i.e. pyrocarbon, and most likely to the presence of defects in the volume of the composites. The velocity of ultrasonic wave propagation in a material is determined by the microstructure of the material. Any discontinuities in the microstructure such as cracks or pores cause reflection, deflection or refraction, i.e. scattering of the ultrasonic wave. Also, the shape and orientation of the pores affects the velocity of the wave. Pores oriented with their longer dimension perpendicular to the direction of ultrasonic wave propagation cause a decrease in velocity to a greater extent than pores oriented with their longer dimension parallel to the direction of wave propagation. This is related to the previously mentioned stress concentration at the grain-pore boundary. As a result, the porosity and shape of the pores cause a greater or a lesser decrease in the value of the ultrasonic wave velocity [62]. Analysing SEM images of the cross-sectional surfaces of composites indicate the presence of defects, e.g. in the form of pores (Fig. 11). As well as in the form of longitudinal and transverse laminar PyC layers. This is particularly noticeable in samples heat treated at higher temperatures. The presence of these defects also translates into a successive decrease in Young's modulus with increasing temperature (Fig. 10). Such microstructural characteristics may contribute to the mechanical weakening of the material, which is supported in the literature [50].

Therefore, based on the results obtained, and in particular the possibility of creating and spreading defects in the volume of the composites, which may contribute to faster degradation of the samples, the most suitable composites for further research in the context of electrodes for stimulation of nervous tissue were obtained at a synthesis temperature of 1100 °C.

4. Conclusions

This study investigated the effects of additional heat treatment on the correlations between microstructure, structure, texture, and stiffness of pyrolytic carbon (CF/PyC) matrix fibre composites. The CF/PyC composites were obtained using an innovative CVD method with direct heating of a carbon fibre bundle.

Methane pyrolysis was used to achieve a homogeneous and partially crystalline pyrolytic carbon matrix. Morphological studies have indicated that heat treatments are a significant factor in maintaining the

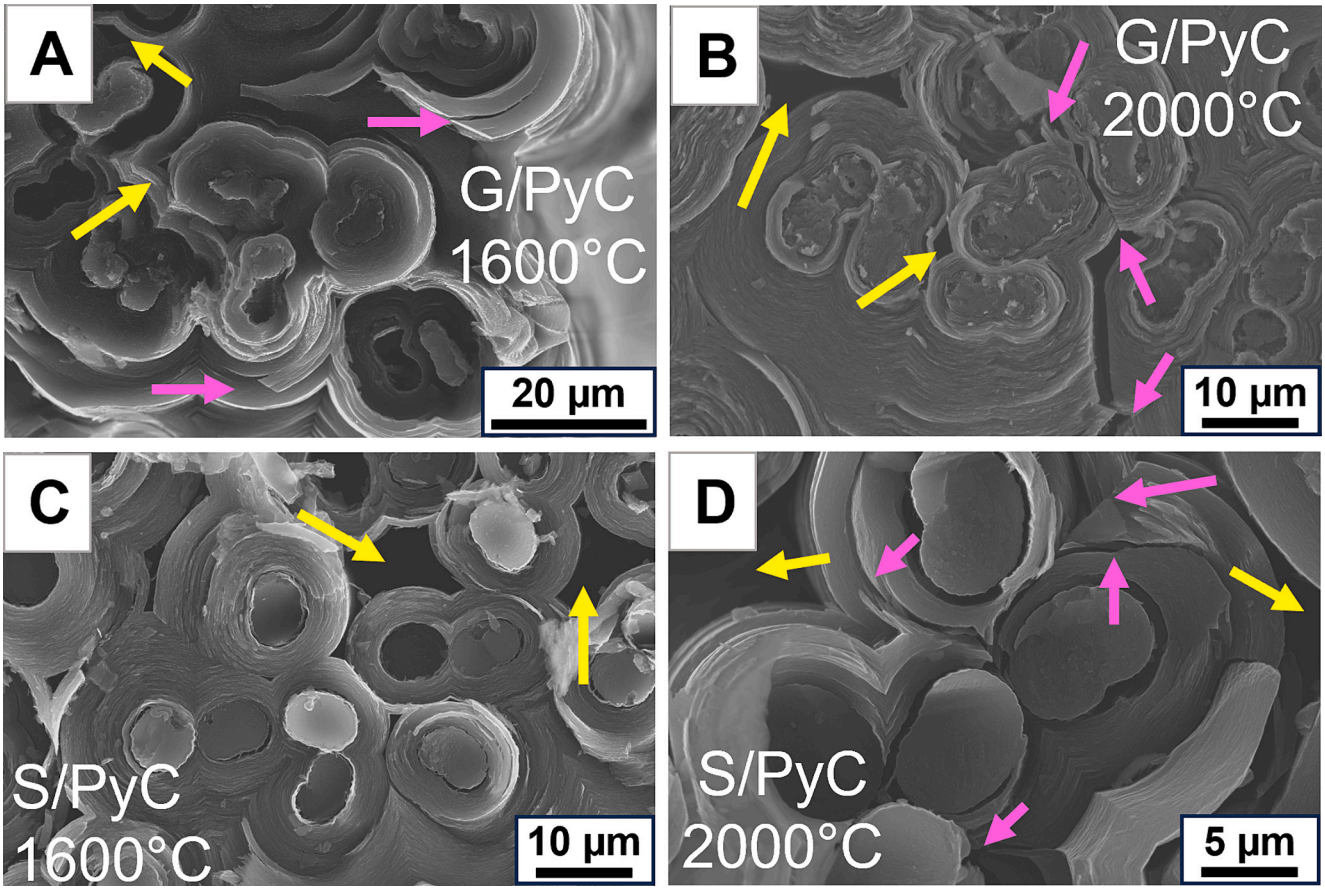

Fig. 11. SEM microphotographs showing microstructural defects at the CF/PyC interface, longitudinally and perpendicular to PyC laminar layers, as well as the presence of non-regular closed pores.

integrity of the phases and interface at the fibre-matrix interface. While the boundary is typically continuous, local microstructural defects produced as a function of heat treatment temperature had a negative impact on the resulting values of dynamic Young's modulus. Furthermore, additional studies have uncovered variations in structure among the studied CFs. It was observed that CF-S underwent a significant graphitisation trajectory with increasing treatment temperature, resulting in carbon structure and crystallite growth. In contrast, CF-G did not undergo any significant further graphitisation with increasing treatment temperature. While the surface area of the carbon fibre can be significant during the deposition of initial PyC layers, this is negligible when compared to the total volume of the matrix. The matrices obtained in both S/PyC and G/PyC are comparable with individual variations due to the nature of PyC. The matrix area distinguished low-textural (LT) and medium-textural (MT) PyC, for which the orientation angles (OA) were affected regardless of the fibre used or the temperature of the final processing.

Analyses of the temperature function of texture evolution, crystallinity growth, crystallisation trajectories, and changes in interplanar spacings indicate similarity. Further considerations reveal a tendency for PyC crystallite growth and an increase in the presence of crystallites, without a significant increase in ordering. It has been observed that changes in the ordering of kinetics are only observed at a temperature of 2000 °C and above. At 1600 °C, it has been noted that amorphous forms may evolve towards turbostratic ones and crystallite growth may begin, but the kineticism is highly limited under these conditions. It is suggested that the major mechanism of the trajectory of graphitisation as a function of the temperatures studied, was the growth of the formed and specifically oriented domains. This mechanism applied to individual pseudo-crystallites and crystallites, rather than the entire pyrocarbon system as a layer. The determined parameters of the average size of crystallites (L_a and L_c) support this hypothesis, where the changes are significant and indicate local graphitisation.

Based on the aforementioned research, it was found that additional heat treatment at temperatures up to 2000 °C of composites obtained at 1100 °C, did not significantly affect the overall structural changes. Moreover, the effect of temperature weakens the mechanical properties of the composite through the development of longitudinal and transverse micro-cracks at the interface between phases and close laminar PyC layers. Thus, notwithstanding the type of carbon fibre used, it has a negligible effect on the differentiation of the structure of the PyC produced. Similar forms of PyC were achieved throughout the matrix. It was also shown that the type of carbon fibre used does not have a significant impact on the mechanical value of the Young's modulus of the obtained C/C composites. In general, economic, energy and time-consuming considerations of additional heat treatment at 1600 and 2000 °C of CF/PyC composites are not worthwhile. Therefore, for the reasons given, it is believed that the most advantageous and promising rod-shaped microelectrode composites for further medical applications are those obtained at 1100 °C.

CRediT authorship contribution statement

Ryszard Wielowski: Writing – review & editing, Writing – original draft, Visualization, Methodology, Investigation, Conceptualization. **Paweł Czaja:** Visualization, Investigation. **Wojciech Piekarczyk:** Methodology, Investigation. **Marcel Zambrzycki:** Methodology, Data curation. **Maciej Gubernat:** Methodology, Investigation. **Aneta Fraczek-Szczypta:** Writing – review & editing, Writing – original draft, Supervision, Project administration, Methodology, Investigation, Funding acquisition, Formal analysis, Data curation, Conceptualization.

Declaration of competing interest

The authors declare the following financial interests/personal relationships which may be considered as potential competing interests: Aneta Fraczek-Szczypta reports financial support was provided by National Science Centre Poland. If there are other authors, they declare that they have no known competing financial interests or personal relationships that could have appeared to influence the work reported in this paper.

Data availability

Data will be made available on request.

Acknowledgements

This research was funded in whole by National Science Centre, Poland, grant number: UMO-2020/39/B/ST5/02126. Hybrid carbon composites for stimulation of cells of the central nervous system.

Appendix A. Supplementary data

Supplementary data to this article can be found online at https://doi.org/10.1016/j.diamond.2024.111214.

References

[1] B.C. Banerjee, T.J. Hirt, P.L. Walker, Pyrolytic carbon formation from carbon suboxide, Nature 192 (1961) 450–451, https://doi.org/10.1038/192450a0.
[2] V.L. Gott, D.E. Alejo, D.E. Cameron, Mechanical heart valves: 50 years of evolution, Ann. Thorac. Surg. 76 (2003) S2230–S2239, https://doi.org/10.1016/j.athoracsur.2003.09.002.
[3] C.L. Renschler, A.P. Sylwester, Conductive, spin-cast carbon films from polyacrylonitrile, Appl. Phys. Lett. 50 (1987) 1420–1422, https://doi.org/10.1063/1.97841.
[4] J.H. Je, J.Y. Lee, A study on the deposition of pyrolytic carbons from hydrocarbons, Carbon N Y 22 (1984) 563–570, https://doi.org/10.1016/0008-6223(84)90090-3.
[5] W.S. Baek, J.-Y. Lee, S.M. Oh, Mechanism of deposition of laminar pyrolytic carbon deposited in a tumbling bed, J. Anal. Appl. Pyrolysis 9 (1986) 247–254, https://doi.org/10.1016/0165-2370(86)80014-6.
[6] M.-H. Kim, J.-Y. Lee, The primary factors which determine the microstructures of pyrolytic carbons deposited in a tumbling bed, J. Mater. Sci. 22 (1987) 3983–3988, https://doi.org/10.1007/BF01133348.
[7] S. Jasieńko, J. Machnikowski, Studies on pyrolytic carbons obtained by acetylene pyrolysis at 1273 K—II, Carbon N Y 19 (1981) 205–208, https://doi.org/10.1016/0008-6223(81)90044-0.
[8] C. Huo, L. Guo, A. Cao, Z. Wang, C. Wang, G. Kou, Y. Zhang, The degradation behavior of C/C composites in high-energy atomic oxygen, Vacuum 146 (2017) 120–129, https://doi.org/10.1016/j.vacuum.2017.09.043.
[9] M. Oliaei, M. Yousefi, Synthesis of pyrolytic carbon from polyethylene terephthalate on graphite substrate, in: Eco-Friendly and Smart Polymer Systems, Springer International Publishing, Cham, 2020, pp. 533–536, https://doi.org/10.1007/978-3-030-45085-4_129.
[10] S. Feng, L. Xu, L. Li, S. Bai, X. Yang, X. Zhou, Sealing nuclear graphite with pyrolytic carbon, J. Nucl. Mater. 441 (2013) 449–454, https://doi.org/10.1016/j.jnucmat.2013.06.035.
[11] R.D. Boehm, C. Jin, R.J. Narayan, Carbon and diamond, in: Comprehensive Biomaterials, Elsevier, 2011, pp. 109–126, https://doi.org/10.1016/B978-0-08-055294-1.00018-0.
[12] J. Stanley, J. Klawitter, R. More, Replacing joints with pyrolytic carbon, in: Joint Replacement Technology, Elsevier, 2008, pp. 631–656, https://doi.org/10.1533/9781845694807.4.631.
[13] R.J. Price, J.C. Bokros, K. Koyama, J. Chin, Structure and properties of pyrolytic carbons prepared in a fluidized bed between 1900° and 2400°C, Carbon N Y 4 (1966) 263–272, https://doi.org/10.1016/0008-6223(66)90088-1.
[14] R.J. Bard, H.R. Baxman, J.P. Bertino, J.A. O'Rourke, Pyrolytic carbons deposited in fluidized beds at 1200 to 1400 °C from various hydrocarbons, Carbon N Y 6 (1968) 603–616, https://doi.org/10.1016/0008-6223(68)90004-3.
[15] J.C. Bokros, R.J. Price, Deformation and fracture of pyrolytic carbons deposited in a fluidized bed, Carbon N Y 3 (1966) 503–519, https://doi.org/10.1016/0008-6223(66)90036-4.
[16] A. Li, S. Zhang, B. Reznik, S. Lichtenberg, G. Schoch, O. Deutschmann, Chemistry and kinetics of chemical vapor deposition of pyrolytic carbon from ethanol, Proc. Combust. Inst. 33 (2011) 1843–1850, https://doi.org/10.1016/j.proci.2010.06.037.
[17] S.S. Sigaeva, V.A. Likholobov, P.G. Tsyrul'nikov, Pyrolysis of methane on a heat-treated FeCrAl coil heated with electric current, Kinet. Catal. 54 (2013) 199–206, https://doi.org/10.1134/S0023158413010126.
[18] X. Xu, T. Ouyang, L. Zeng, L. Chai, Study on the pyrolytic carbon generated by the electric heating CVD method, Journal of Wuhan University of Technology-Mater. Sci. Ed. 33 (2018) 409–413, https://doi.org/10.1007/s11595-018-1837-4.
[19] A. Fraczek-Szczypta, N. Kondracka, M. Zambrzycki, M. Gubernat, P. Czaja, M. Pawlyta, P. Jelen, R. Wielowski, D. Jantas, Exploring CVD method for

synthesizing carbon–carbon composites as materials to contact with nerve tissue, J Funct Biomater 14 (2023) 443, https://doi.org/10.3390/jfb14090443.
[20] C. Guéret, M. Daroux, F. Billaud, Methane pyrolysis: thermodynamics, Chem. Eng. Sci. 52 (1997) 815–827, https://doi.org/10.1016/S0009-2509(96)00444-7.
[21] S.D. Robertson, Graphite formation from low temperature pyrolysis of methane over some transition metal surfaces, Nature 221 (1969) 1044–1046, https://doi.org/10.1038/2211044a0.
[22] S. Bammidipati, G.D. Stewart, J.R. Elliott, S.A. Gokoglu, M.J. Purdy, Chemical vapor deposition of carbon on graphite by methane pyrolysis, AICHE J. 42 (1996) 3123–3132, https://doi.org/10.1002/aic.690421112.
[23] P. Lucas, A. Marchand, Pyrolytic carbon deposition from methane: an analytical approach to the chemical process, Carbon N Y 28 (1990) 207–219, https://doi.org/10.1016/0008-6223(90)90115-F.
[24] F. Larkins, A. Khan, Pyrolysis of methane to higher hydrocarbons: a thermodynamic study, Aust. J. Chem. 42 (1989) 1655, https://doi.org/10.1071/CH9891655.
[25] C. Hu, H. Shen, S. Zhang, H. Li, Methane pyrolysis in preparation of pyrolytic carbon: thermodynamic and kinetic analysis by density functional theory, Chin. J. Aeronaut. 33 (2020) 1064–1073, https://doi.org/10.1016/j.cja.2019.02.015.
[26] M.W. Chen, Y.B. Zhu, J. Xia, H.A. Wu, Molecular insights into the initial formation of pyrolytic carbon upon carbon fiber surface, Carbon N Y 148 (2019) 307–316, https://doi.org/10.1016/j.carbon.2019.04.003.
[27] P.J. Meadows, E. López-Honorato, P. Xiao, Fluidized bed chemical vapor deposition of pyrolytic carbon – II. Effect of deposition conditions on anisotropy, Carbon N Y 47 (2009) 251–262, https://doi.org/10.1016/j.carbon.2008.10.003.
[28] O.V. Belyaeva, T.A. Krasnova, O.S. Gladkova, Effect of the thermal treatment conditions of granulated active carbons on their properties, Solid Fuel Chemistry 49 (2015) 196–200, https://doi.org/10.3103/S0361521915030040.
[29] S. Kumar, R. Kumar, Influence of processing conditions on the properties of thermal sprayed coating: a review, Surf. Eng. 37 (2021) 1339–1372, https://doi.org/10.1080/02670844.2021.1967024.
[30] H. Zhang, E. López-Honorato, P. Xiao, Fluidized bed chemical vapor deposition of pyrolytic carbon-III. Relationship between microstructure and mechanical properties, Carbon N Y 91 (2015) 346–357, https://doi.org/10.1016/j.carbon.2015.05.009.
[31] I.Y. Stein, A.J. Constable, N. Morales-Medina, C.V. Sackier, M.E. Devoe, H. M. Vincent, B.L. Wardle, Structure-mechanical property relations of non-graphitizing pyrolytic carbon synthesized at low temperatures, Carbon N Y 117 (2017) 411–420, https://doi.org/10.1016/j.carbon.2017.03.001.
[32] J.H. Richardson, E.H. Zehms, Structural Changes in Pyrolytic Graphite at Elevated Temperatures, 1963, https://doi.org/10.21236/AD0427346.
[33] L. Blackman, G. Saunders, A. Ubbelohde, Defect structure and properties of pyrolytic carbons, Proc. R. Soc. Lond. A Math. Phys. Sci. 264 (1961) 19–40, https://doi.org/10.1098/rspa.1961.0183.
[34] J.C. Bokros, R.J. Price, T.A. Trozera, Influence of structure on mechanical properties of pyrolytic carbon, Nature 204 (1964) 371–372, https://doi.org/10.1038/204371a0.
[35] V. De Pauw, S. Kalhöfer, D. Gerthsen, Influence of the deposition parameters on the texture of pyrolytic carbon layers deposited on planar substrates, Carbon N Y 42 (2004) 279–286, https://doi.org/10.1016/j.carbon.2003.10.027.
[36] Y. Ohzawa, M. Mitani, J. Li, T. Nakajima, Structures and electrochemical properties of pyrolytic carbon films infiltrated from gas phase into electro-conductive substrates derived from wood, Mater. Sci. Eng. B 113 (2004) 91–98, https://doi.org/10.1016/j.mseb.2004.07.006.
[37] E. López-Honorato, P.J. Meadows, P. Xiao, Fluidized bed chemical vapor deposition of pyrolytic carbon – I. Effect of deposition conditions on microstructure, Carbon N Y 47 (2009) 396–410, https://doi.org/10.1016/j.carbon.2008.10.023.
[38] A. Fraczek-Szczypta, Carbon nanomaterials for nerve tissue stimulation and regeneration, Mater. Sci. Eng. C 34 (2014) 35–49, https://doi.org/10.1016/j.msec.2013.09.038.
[39] Y. Huang, R.J. Young, Effect of fibre microstructure upon the modulus of PAN- and pitch-based carbon fibres, Carbon N Y 33 (1995) 97–107, https://doi.org/10.1016/0008-6223(94)00109-D.
[40] M. Guigon, A. Oberlin, G. Desarmot, Microtexture and structure of some high-modulus, PAN-base carbon fibres, Fibre Science and Technology 20 (1984) 177–198, https://doi.org/10.1016/0015-0568(84)90040-X.
[41] M. Wojdyr, Fityk: a general-purpose peak fitting program, J. Appl. Crystallogr. 43 (2010) 1126–1128, https://doi.org/10.1107/S0021889810030499.
[42] M. Zambrzycki, R. Piech, S.R. Raga, M. Lira-Cantu, A. Fraczek-Szczypta, Hierarchical carbon nanofibers/carbon nanotubes/NiCo nanocomposites as novel highly effective counter electrode for dye-sensitized solar cells: a structure-electrocatalytic activity relationship study, Carbon N Y 203 (2023) 97–110, https://doi.org/10.1016/j.carbon.2022.11.047.
[43] A.N. Popova, Crystallographic analysis of graphite by X-ray diffraction, Coke Chem. 60 (2017) 361–365, https://doi.org/10.3103/S1068364X17090058.
[44] M. Drescher, K.J. Hüttinger, E. Dormann, Pyrolytic carbon layers—an electron spin resonance analysis, Carbon N Y 41 (2003) 773–783, https://doi.org/10.1016/S0008-6223(02)00397-4.
[45] Y.-G. He, K.-Z. Li, H.-J. Li, J.-F. Wei, Q.-G. Fu, D.-S. Zhang, Effect of interface structures on the fracture behavior of two-dimensional carbon/carbon composites by isothermal chemical vapor infiltration, J. Mater. Sci. 45 (2010) 1432–1437, https://doi.org/10.1007/s10853-009-4089-0.
[46] J. Piekarczyk, H.W. Hennicke, R. Pampuch, On determining the elastic constants of porous zinc ferrite materials, Cfi/Ber. D.K.G. 59 (1982) 227–232.
[47] B. Reznik, K. Norinaga, D. Gerthsen, O. Deutschmann, The effect of cooling rate on hydrogen release from a pyrolytic carbon coating and its resulting morphology, Carbon N Y 44 (2006) 1330–1334, https://doi.org/10.1016/j.carbon.2005.12.014.
[48] M.S.A. Rahaman, A.F. Ismail, A. Mustafa, A review of heat treatment on polyacrylonitrile fiber, Polym. Degrad. Stab. 92 (2007) 1421–1432, https://doi.org/10.1016/j.polymdegradstab. 2007.03.023.
[49] J. Tezcan, S. Ozcan, B. Gurung, P. Filip, Measurement and analytical validation of interfacial bond strength of PAN-fiber-reinforced carbon matrix composites, J. Mater. Sci. 43 (2008) 1612–1618, https://doi.org/10.1007/s10853-007-2333-z.
[50] S.-S. Tzeng, Y.-G. Chr, Evolution of microstructure and properties of phenolic resin-based carbon/carbon composites during pyrolysis, Mater. Chem. Phys. 73 (2002) 162–169, https://doi.org/10.1016/S0254-0584(01)00358-3.
[51] Y. Ohzawa, T. Okabe, T. Kasugai, T. Nakajima, Pyrolytic carbon coating on carbon paper carbonized at 800 °C and its anode property for lithium-ion battery, Carbon N Y 49 (2011) 1508, https://doi.org/10.1016/j.carbon.2010.11.021.
[52] R.H. Bragg, Y. Hishiyama, A. Yoshida, Y. Kaburagi, The presence of multiple structural components in pyrolytic carbon at the deposition stage, Carbon N Y 74 (2014) 367–369, https://doi.org/10.1016/j.carbon.2014.03.018.
[53] Z. Hua, Y. Yang, Y. Zhong, D. Li, X. Liu, Characterization and properties of PAN-based high modulus carbon fibers, Carbon N Y 48 (2010) 314, https://doi.org/10.1016/j.carbon.2009.09.019.
[54] B. Reznik, D. Gerthsen, K.J. Hüttinger, Micro- and nanostructure of the carbon matrix of infiltrated carbon fiber felts, Carbon N Y 39 (2001) 215–229, https://doi.org/10.1016/S0008-6223(00)00116-0.
[55] R.J. Price, J.C. Bokros, K. Koyama, Thermal expansivities and preferred orientation of pyrolytic carbons, Carbon N Y 5 (1967) 423–430, https://doi.org/10.1016/0008-6223(67)90018-8.
[56] M. Gubernat, M. Zambrzycki, A. Fraczek-Szczypta, S. Blazewicz, Structural and microstructural study of novel stacked toroidal carbon nanotubes, Micron 130 (2020) 102816, https://doi.org/10.1016/j.micron.2019.102816.
[57] A. Sadezky, H. Muckenhuber, H. Grothe, R. Niessner, U. Pöschl, Raman microspectroscopy of soot and related carbonaceous materials: spectral analysis and structural information, Carbon N Y 43 (2005) 1731–1742, https://doi.org/10.1016/j.carbon.2005.02.018.
[58] A.C. Ferrari, J. Robertson, Interpretation of Raman spectra of disordered and amorphous carbon, Phys. Rev. B 61 (2000) 14095–14107, https://doi.org/10.1103/PhysRevB.61.14095.
[59] G.L. Dong, K.J. Hüttinger, Consideration of reaction mechanisms leading to pyrolytic carbon of different textures, Carbon N Y 40 (2002) 2515–2528, https://doi.org/10.1016/S0008-6223(02)00174-4.
[60] Z.J. Hu, K.J. Hüttinger, Mechanisms of carbon deposition—a kinetic approach, Carbon N Y 40 (2002) 624–628, https://doi.org/10.1016/S0008-6223(01)00316-5.
[61] G.L. Vignoles, F. Langlais, C. Descamps, A. Mouchon, H. Le Poche, N. Reuge, N. Bertrand, CVD and CVI of pyrocarbon from various precursors, Surf. Coat. Technol. 188–189 (2004) 241–249, https://doi.org/10.1016/j.surfcoat.2004.08.036.
[62] O. Yousefian, R.D. White, Y. Karbalaeisadegh, H.T. Banks, M. Muller, The effect of pore size and density on ultrasonic attenuation in porous structures with monodisperse random pore distribution: a two-dimensional in-silico study, J. Acoust. Soc. Am. 144 (2018) 709–719, https://doi.org/10.1121/1.5049782.